Modelling and analysis of crack turning on aeronautical structures

Llorenç Llopart Prieto

Modelling and analysis of crack turning on aeronautical structures

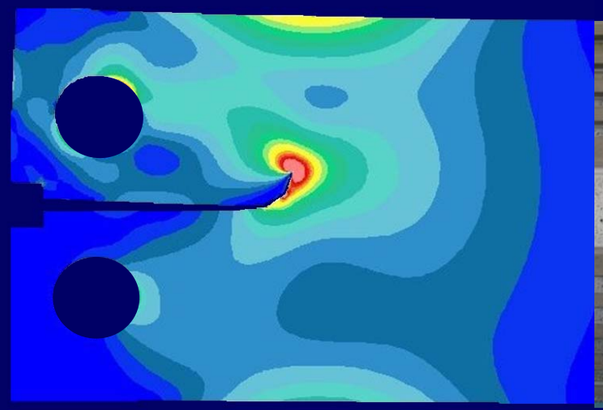

Doctoral Thesis

Llorenç Llopart Prieto

Director:
Dr. Marc Anglada i Gomila

Departament de Ciència dels Materials i Enginyeria Metal·lúrgica
UNIVERSITAT POLITÈCNICA DE CATALUNYA

Company director:
Elke Hombergsmeier

EADS
European Aeronautical Defence and Space company

EADS

UNIVERSITAT POLITÈCNICA DE CATALUNYA

UPC

EADS

Ottoburnn / Barcelona April 2007

4 Experimental testing

This chapter introduces the materials, the special characterisation techniques and the experimental testing, which were used during this work. On section 4.3 the used specimens, tests set-ups and results are described.

4.1 Materials

Conventional and relatively new-developed heat-treatable aluminium alloys for aircraft industry were used in the analyses performed within this doctoral thesis. These are the aluminium alloy 2024-T3 and 6013-T6, whose chemical composition is described in Tables 4.1 and 4.2, respectively.

Table 4.1. Chemical composition of the AA 2024-T3 sheet [S2]

Element	***Si***	***Fe***	***Cu***	***Mn***	***Mg***	***Cr***	***Zn***	***Ti***	***Ti+Zr***	***Other***		***Al***
										Each	***Total***	
Min [Wt%]	-	-	3.80	0.30	1.20	-	-	-	-	-	-	Base
Max [Wt%]	0.50	0.50	4.90	0.90	1.80	0.10	0.25	0.15	-	0.05	0.15	

As already introduced in section 2.1.1, the alloy *AA* 2024-T3 has been used since more than 30 years on aircraft constructions due to its positive combination on strength, damage-tolerance and its relatively low manufacturing costs. On the other hand, the aluminium alloy 6013-T6 provides high strength together with good toughness. Moreover, it offers excellent corrosion resistance and weldability.

Table 4.2. Chemical composition of the AA 6013-T6 [S4]

Element	***Si***	***Fe***	***Cu***	***Mn***	***Mg***	***Cr***	***Zn***	***Ti***	***Ti+Zr***	***Other***		***Al***
										Each	***Total***	
Min [Wt%]	0.60	-	0.15	0.20	0.60	-	0.10	-	-	-	-	Base
Max [Wt%]	1.30	0.50	1.10	1.00	1.20	0.25	0.70	0.10	0.20	0.05	0.15	

Sheet aluminium alloy 2024-T3 was delivered by Airbus Deutschland GmbH and aluminium alloy 6013-T6 was acquired from Otto Fuchs KG under two stringer profile form.

4.2. Special characterisation techniques

This section provides an insight on special applied measuring techniques which has been used to characterise the materials. These are the direct current potential drop method for the calculation of the crack length and the ARAMIS system for the evaluation of the strain/stress field distributions in-situ during testing.

During this work, standard characterisation testing methods according to ASTM E399 [S3], ASTM E647 [S5], EN 10002 [S6] have been used.

Besides, a light microscope Leica Polyvar SC, was used to find out the extrusion direction of the delivered sheet *AA* 2024-T3. And, a scanning electron microscope type LEO 1430 fitted out with the picture processing and archiving software "image Access" was used to study the fracture surfaces of the broken *2SP*-specimens.

4.2.1 The direct current potential drop method

Crack propagation on metallic materials under static or cyclic loading can be measured automatically by the direct current potential drop method. This method is based on the feature that the resistance of a metallic structure is dependent on the specimen geometry. A direct electrical current flow is introduced in the structure as indicated in Figure 4.1.

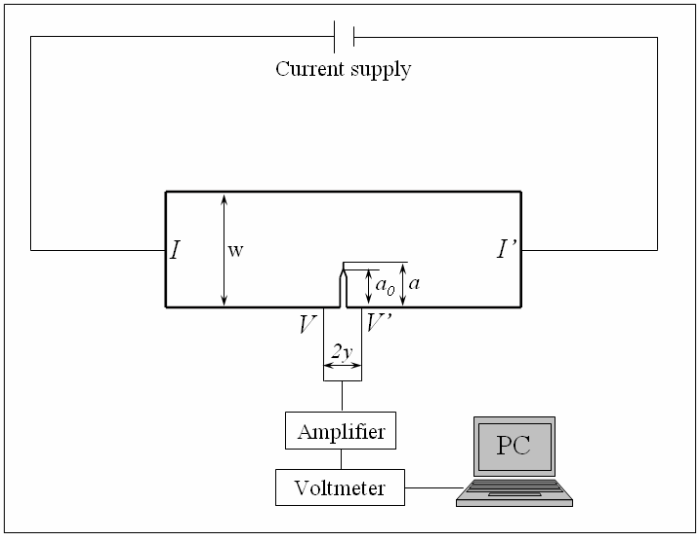

Figure 4.1. Schematic illustration of the current potential drop method

With the growth of the crack, new fracture surfaces are created, but these oxidize immediately under a corrosive environment, for example aluminum in air. The generated oxide film does not conduct the electricity through the crack surfaces, therefore, the conducting cross-section decreases by crack growth, and consequently a potential drop is measured at the crack surroundings, e.g. *V* and *V'* positions.

The relation between the potential drop and the crack growth can be experimentally or analytically calibrated. Usual analytic procedures are the Johnson equation which is valid only for *2D*-configurations, i.e. straight crack fronts, and which is given by,

$$\frac{U}{U_0} = \frac{\cosh^{-1}\left[\cosh\left(\frac{\pi y}{2w}\right) / \cos\left(\frac{\pi a}{2w}\right)\right]}{\cosh^{-1}\left[\cosh\left(\frac{\pi y}{2w}\right) / \cos\left(\frac{\pi a_0}{2w}\right)\right]} \quad \textbf{(4.1)}$$

where w is the specimen width; $2y$ the initial probe spacing; a_0 the initial crack length; U is the variation in electrical potential through the specimen and U_0 is the initial value of the potential.

The equipment used in the measurements, i.e. voltmeter alone or amplifier plus voltmeter, should have a sensitivity to detect potential changes between *0.5* and *5* μV. This allows a measurement of crack lengths within a *5* μm of resolution limit.

4.2.2 Strain mapping system: ARAMIS®

ARAMIS® is a deformation measuring system, which processes and visualizes the images by digital camera in order to obtain an impression of the distribution of strain in the measured object. The surface of interest on the structure to be analysed by ARAMIS® must be provided with a pattern. For example, a black pattern over a white surface can be coloured by means of spray painting. This allows the system to recognise the surface structure in digital image and it is able to allocate the same point in the pattern for different images. First, a reference image has to be stored on an undeformed state. Depending on the type of analysis, a second or more images can be recorded. ARAMIS® compares the position of the points for each image and register any displacement of the object-characteristics in *3D*-coordinates. With the knowledge of the displacement at each point, and by applying the theory of solid mechanics, ARAMIS® can

calculate the different strain values including strain *x*, strain *y*, Von Mises strain, major strain, minor strain and shear strain after image processing. The strain distribution is then shown in a colourful picture.

4.3 Experimental sets and results of testing

During this work, six different set of experiments were carried out. The first and second were a set of standard tests, which were planned to supply material information necessary for the simulation (set reference DE01 and DE02). Part of the results was also used to evaluate the software (set reference DE02). The third set, described in section 4.3.2, was planned to evaluate the capacity of the software to perform crack growth predictions on complex *3D*-structures (set reference DE03). And the last sets (set references RU04, DE05 and RU06), described in section 4.3.3, were planned to evaluate the influence of material anisotropy, loading conditions and notch geometry on the crack turning behaviour. Furthermore, the test results were employed to analyse and develop crack turning criteria by comparing them with the simulation results.

All tests presented in this dissertation were done at room temperature.

4.3.1 Standard tests

Nine standard plane dog-bone tensile specimens were cut from the *AA* 6013-T6 two-stringer profile form in L, *45°* and LT directions as schematised in Figure 4.2.a. This test set is referenced DE01.

Table 4.3. Mechanical properties of 6013-T3 profile

Direction	***E [MPa]***	***$R_{p0.2}$ [MPa]***	***R_m [MPa]***	***A [%]***	***Z [%]***	***r-value [-]***
L	68000	362	382	16	40	0.59
45°	70400	375	408	9	25	0.69
LT	68500	370	410	11	25	0.7

Standard tensile tests, according to EN 10002 [S6], were done with these specimens to obtain the stress-strain curve and therewith the Young's modulus, *E*, the yield tensile strength, $R_{p0.2}$, the ultimate yield tensile strength, R_m, the anisotropy ratio, *r-value*, the elongation, *A*, and the contraction, *Z*, at fracture. The material properties obtained form the test are summarised in Table 4.3 and Figure 4.3.

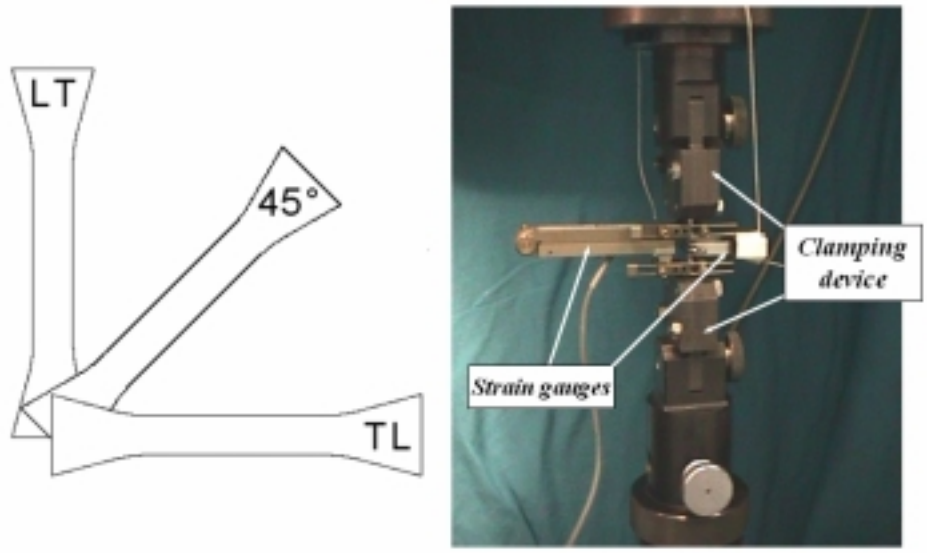

Figure 4.2. a) Standard dog-bone specimens in L, 45° and LT directions, b) test set-up for the specimens in a)

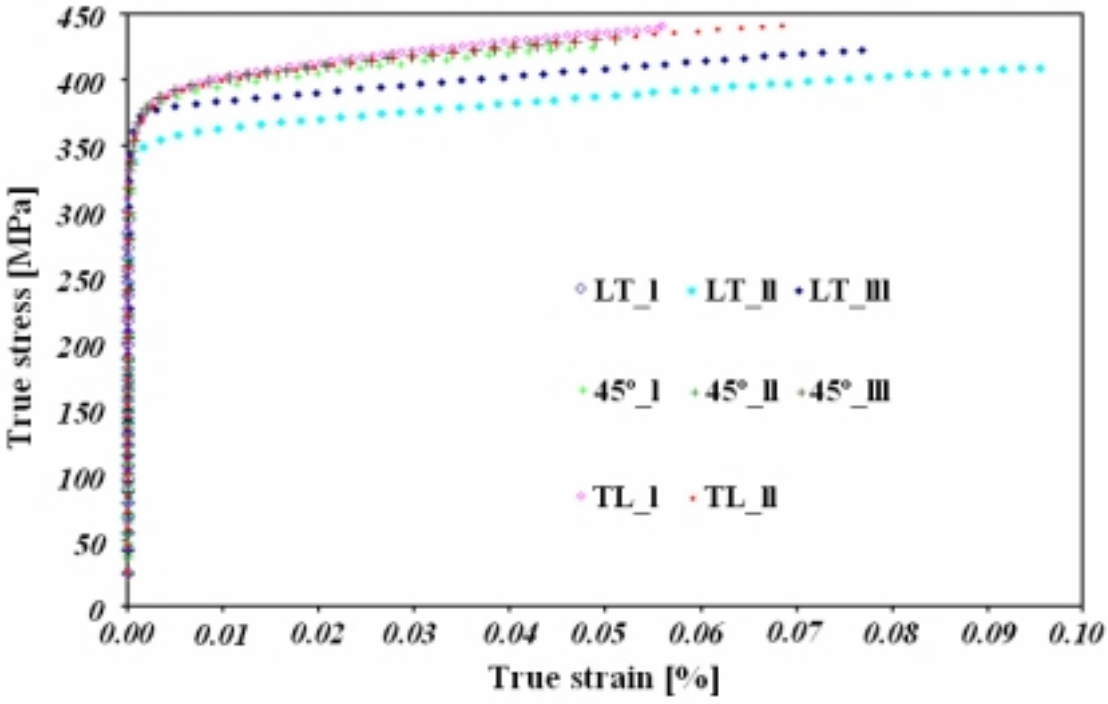

Figure 4.3. True stress-true strain curve for AA6013-T3 L, 45° and LT directions

Thirty-six middle cracked tension (*MT*) specimens, as shown in Figure 4.4, were extracted from the delivered two stringer profile forms to evaluate the crack propagation behaviour and the fracture toughness in the L-T, 45° and T-L directions. Twenty-four specimens where milled to a thickness of *1.6* mm and the rest, i.e. twelve specimens, to *2.5* mm. This test set is referenced DE02.

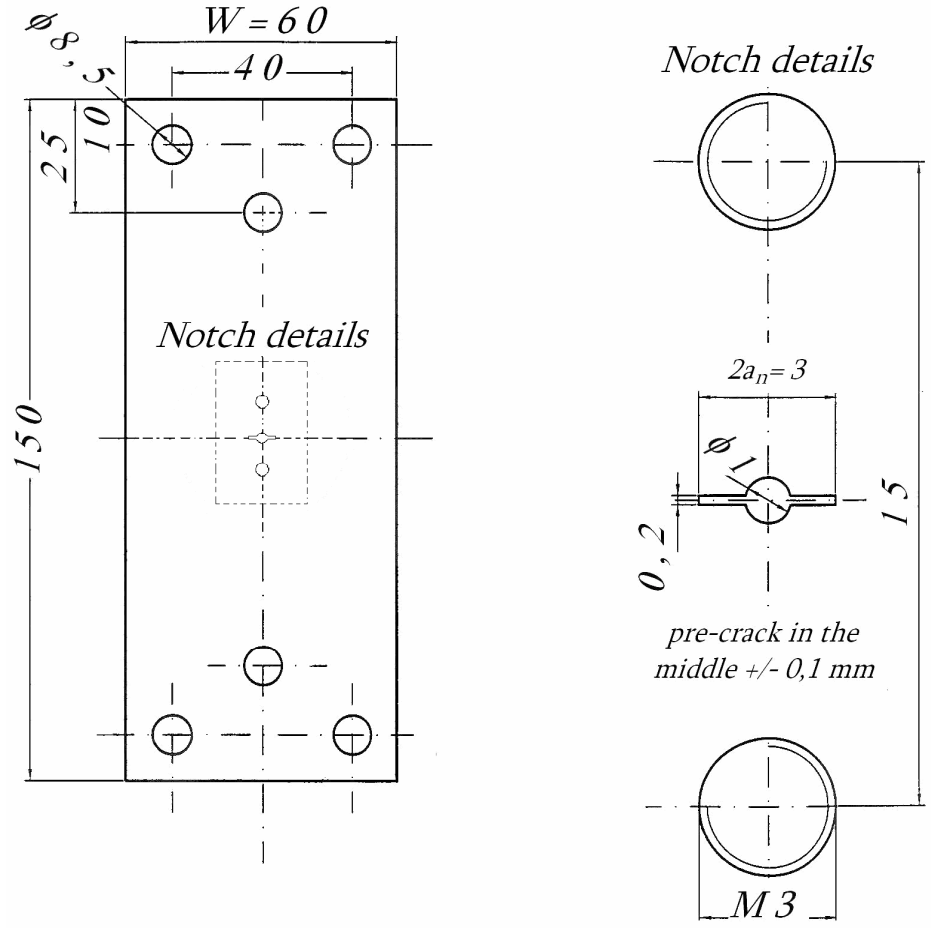

all dimensions in mm

Figure 4.4. Dimensions of the MT-specimen reference DE02

The manufactured specimens were then tested on a servo hydraulic testing machine, INSTRON® Model 8032, with a maximum load capacity of *50* kN. First, a *1* mm fatigue pre-crack was generated at the root of the notch with load ratio, *R*, equal to *0.1* and maximum stresses of *100* and *180* MPa at frequencies of *10* and *5* Hz respectively. Afterwards, crack growth rate tests were performed on these specimens according to *AITM* 1-0042 [S7], which is based on the *ASTM* standard E647 [S5].

During the crack propagation tests, the load ratio and the maximum stresses used were the same as during precracking but the frequencies were reduced to *5* and *2* Hz respectively. The crack was propagated from *5* mm to *20* mm and the growth was monitored by means of the direct current potential drop method and a travelling microscope with a magnification of 50x, as shown in Figure 4.5.

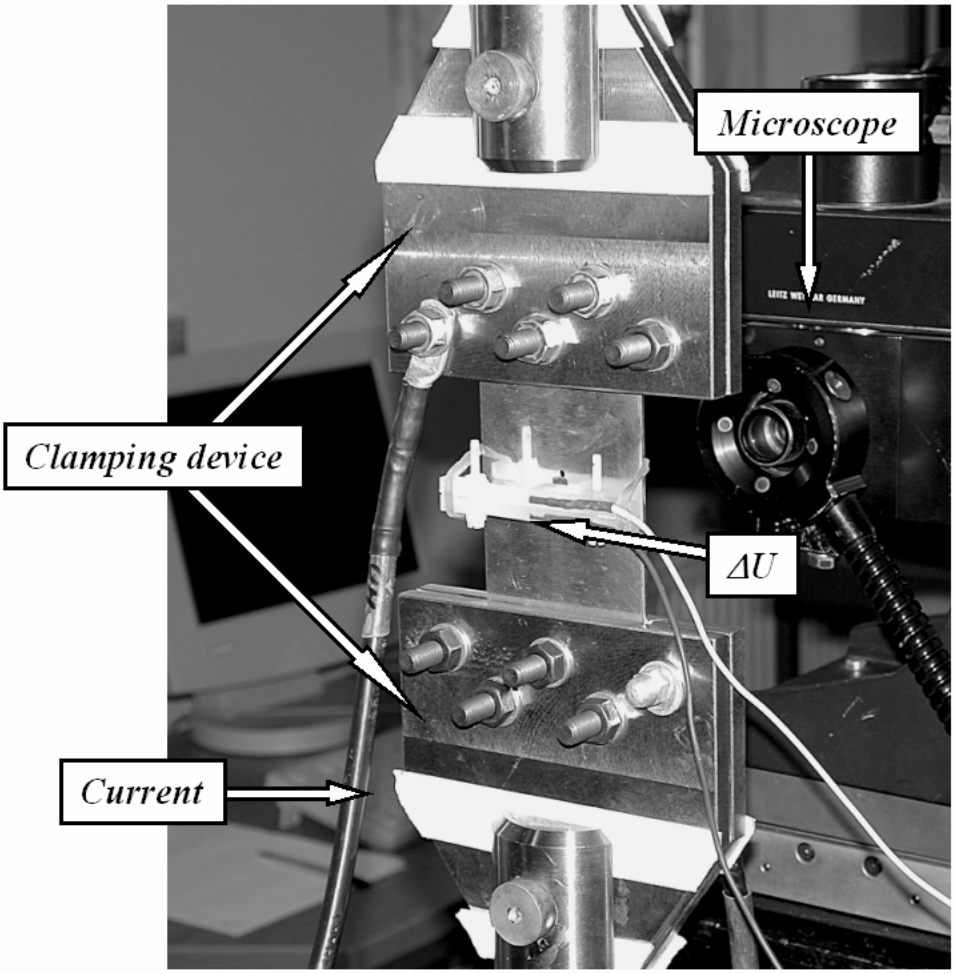

Figure 4.5. MT test-rig reference DE02

The collected crack length data was stored with its corresponding number of cycles, *N*. The fatigue crack growth rate, *da/dN* versus *ΔK*, were then calculated by means of DIAdem® and a routine, the secant method which is described in the annexes of the ASTM standard E647 [S5]. DIAdem® is a programmable software-tool which has the abilities to import, analyse, present and store technical data. The calculation of *ΔK* was done in the routine by using equation 4.2, given in the standards.

$$\Delta K = \frac{\Delta F}{tw}\sqrt{\pi a \sec\frac{\pi a}{2}} \qquad \textbf{(4.2)}$$

where *ΔF* is the difference between maximum and minimum forces at each cycle, *t* is the specimen thickness, *a* the crack length and *w* the width of the specimen. Figures 4.6 and 4.7 show the obtained crack propagation rates after this computational process.

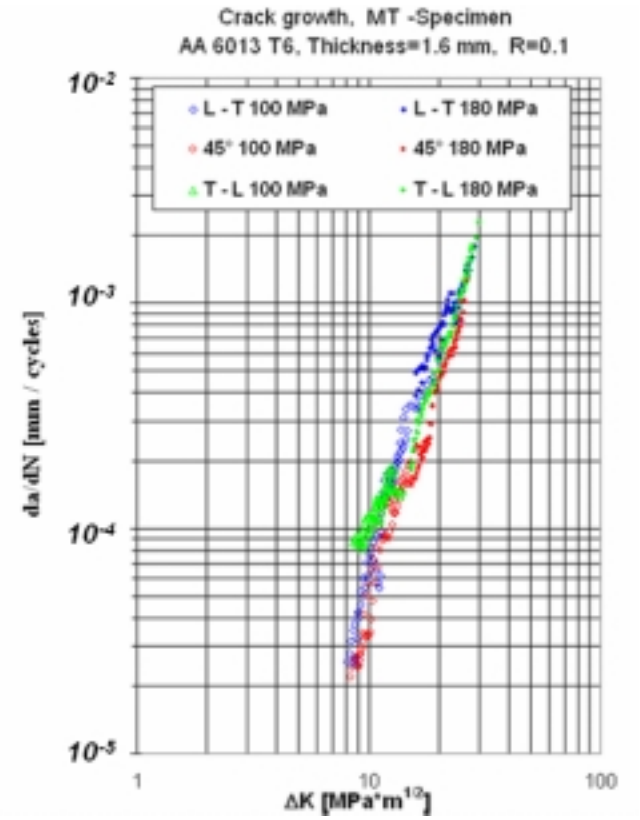

Figure 4.6. Crack growth rate for all MT-specimens with a thickness of 1.6 mm

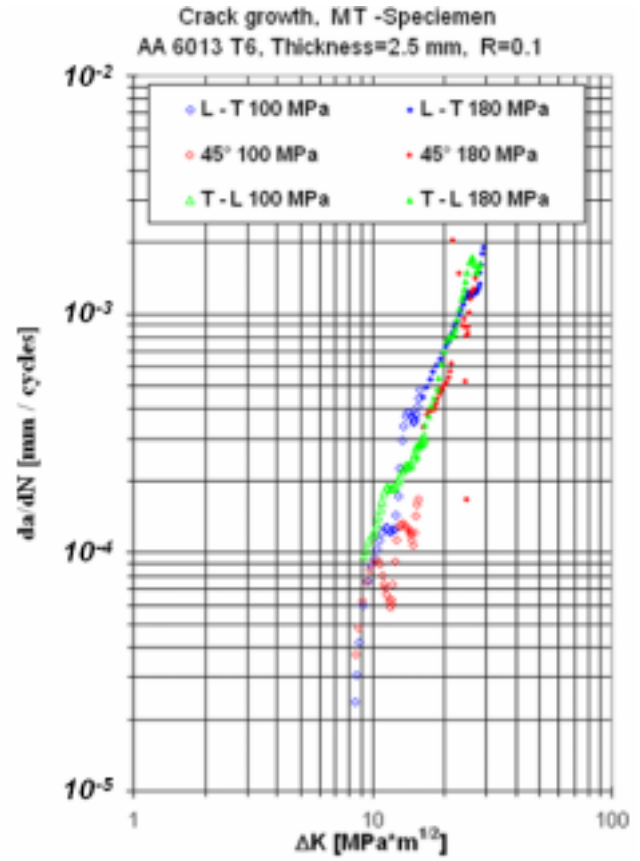

Figure 4.7. Crack growth rate for all MT-specimens with a thickness of 2.5 mm

The specimens with *1.6* mm thickness were further tested under quasi-static loading from the *20* mm cyclic propagated crack. These tests were performed in order to evaluate the fracture toughness according to *ASTM* E399 standard [S3] under a tear speed of *1* mm/min. The results are depicted in Figures 4.8 to 4.10.

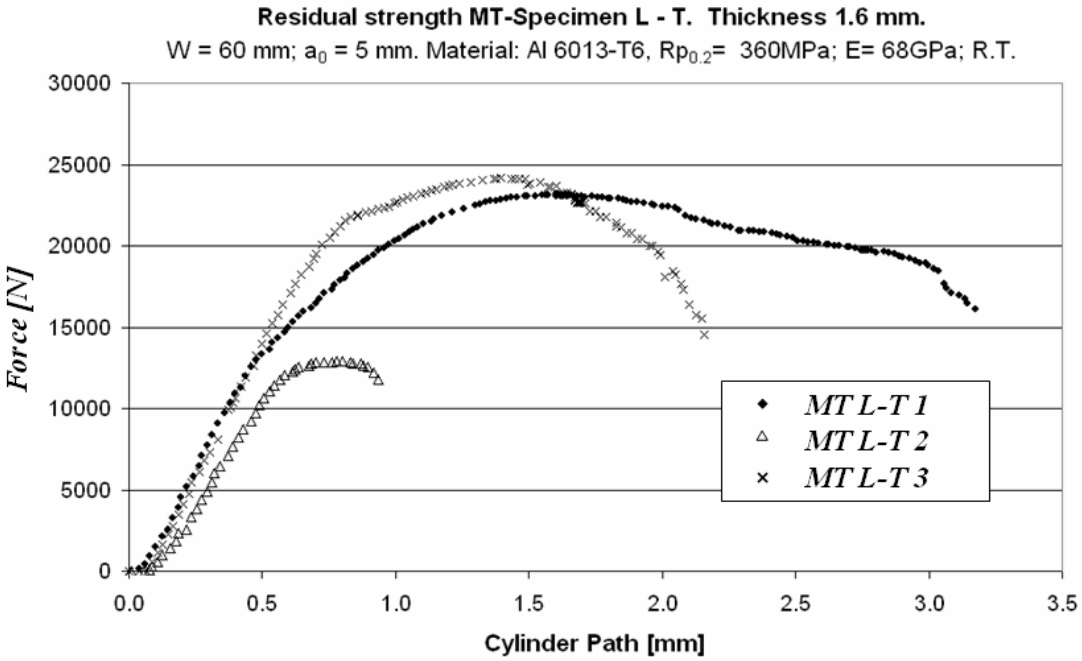

Figure 4.8. Residual strength test curves for L-T specimens

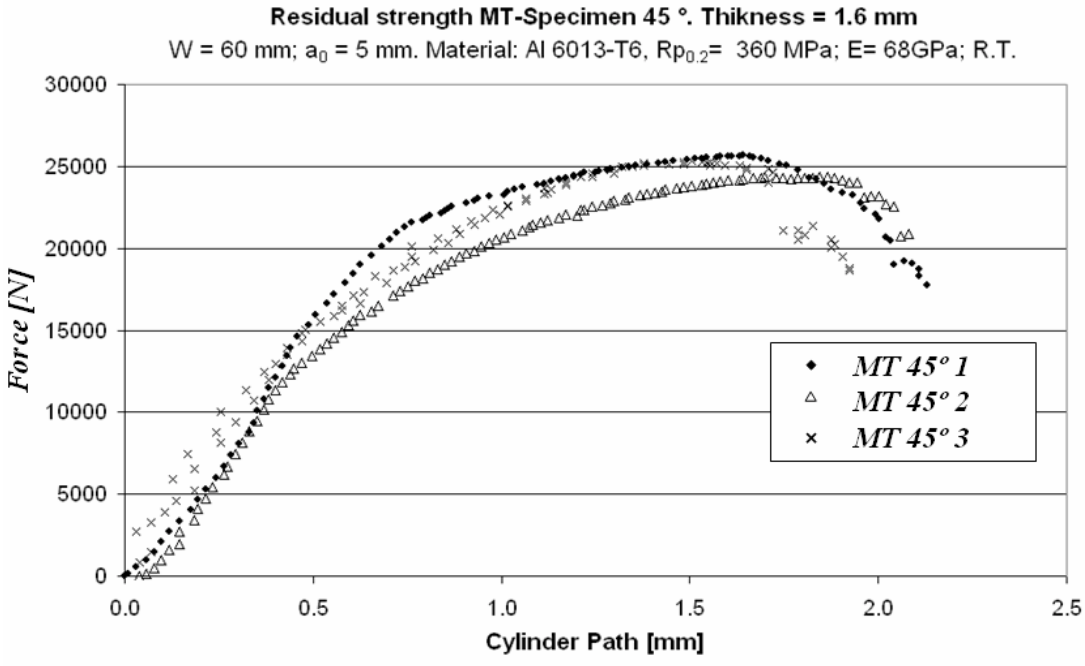

Figure 4.9. Residual strength test curves for 45° direction

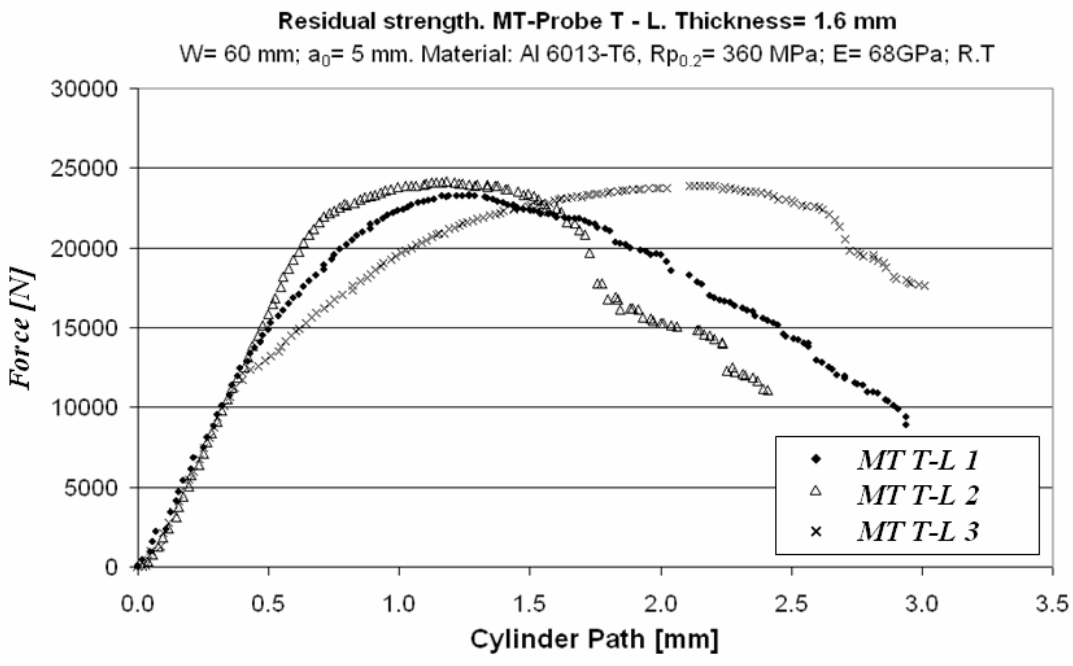

Figure 4.10. Residual strength test curves for T-L specimens

By means of the obtained results and according to *ASTM* E399 the fracture toughnesses for the different sheet directions, K_c, were calculated. These are summarised in Table 4.4.

Table 4.4. Fracture toughness of 6013-T3 profile

Direction	***K_c [MPa*m$^{1/2}$]***
L-T	46
45°	49
T-L	47

Table 4.5. Mechanical properties of 2024-T3 sheet with a thickness between 0.25-3.25 mm

	E [GPa]	***ν [-]***	***$R_{p0.2}$ [MPa]***		***K_{Ic} [MPa*m$^{1/2}$] (pl. strain)***	***K_c [MPa*m$^{1/2}$] (pl. stress)***	***Elongation [%]***	***R_m [MPa]***		***G [GPa]***
			L	***LT***				***L***	***LT***	
MMPDS	71.4	0.33	320-326	286-292	47-30	-	15	435-442	428-435	27.2
AFGROW	71.4	0.33		381	39	110	-	-	-	-
MMPDS Clad	71.4	0.33	306-320	272-286	-	-	-	422-428	415-422	-

Due to the fact that the aluminium alloy 2024-T3 has been widely used, it exists a lot of information about its properties in all its different forms. Therefore no additional tests were carried out since all required information was already available. The mechanical and fracture properties used in this work, were taken from the Airbus Industries Material Specification standard (*AIMS*) [S2], the Metallic Material Properties Development and Standardisation

(*MMPDS*) [S8] and the Air Force crack GROWth software (AFGROW) database [W1]. These properties are summarised in Table 4.5.

4.3.2 The Two-stringer specimen test (set reference DE03)

This test was performed in order to carry out an evaluation on the capacity of the software to perform crack growth predictions on complex *3D*-structures.

The delivered two stringer profile form was machined and modified to the geometry illustrated in Figure 4.11. A pocketing zone of *1.6* mm thickness was created as well as a tear strap of *2.5* mm thick under the stringer. The stringer end and the thickness transitions were rounded in order to avoid stress concentrations that could generate cracks during testing.

In order to avoid failure from the machined holes, the hole-zones were designed to be thicker (*6* mm*)*. In addition, for assuring that the force line remains parallel to the sheet of the specimen and in the middle of the sheet, the thickness was increased in form of four bonded sheet material (dopplers) of *3* mm thickness on both sides, in front and behind, as represented in Figure 4.12. The dopplers were made with the same aluminium alloy as the *2SP*-specimen, i.e. 6013-T6. The bonding took place with a two-component Epoxy resin, M3-DP49, which were mixed and applied by means of a compressed pistol. The curing was done on a press under *200* N during *12* hours at *80* degrees.

The manufactured specimens were then tested with an anti-bending device on a servo hydraulic machine, Schenck® Hydropuls PSB, with a maximum load capacity of *250* kN. A *1* mm fatigue pre-crack was first generated at the root of the notch with a maximum stress of *100* MPa and a frequency of *10* Hz. Afterwards, fatigue crack growth rate tests were performed according to *AITM* 1-0042 [S7].

The applied cyclic loading ratio was *0.1* with a maximal stress of *100* MPa and a frequency of *5* Hz. The crack was propagated from its original length, $2a_0 = 5$ mm, to the failure of the specimen. Unstable crack growth took place after the failure of one of the stringers. During the crack propagation the growth was monitored by means of a travelling microscope, with a magnification of 50x as illustrated in Figure 4.13.

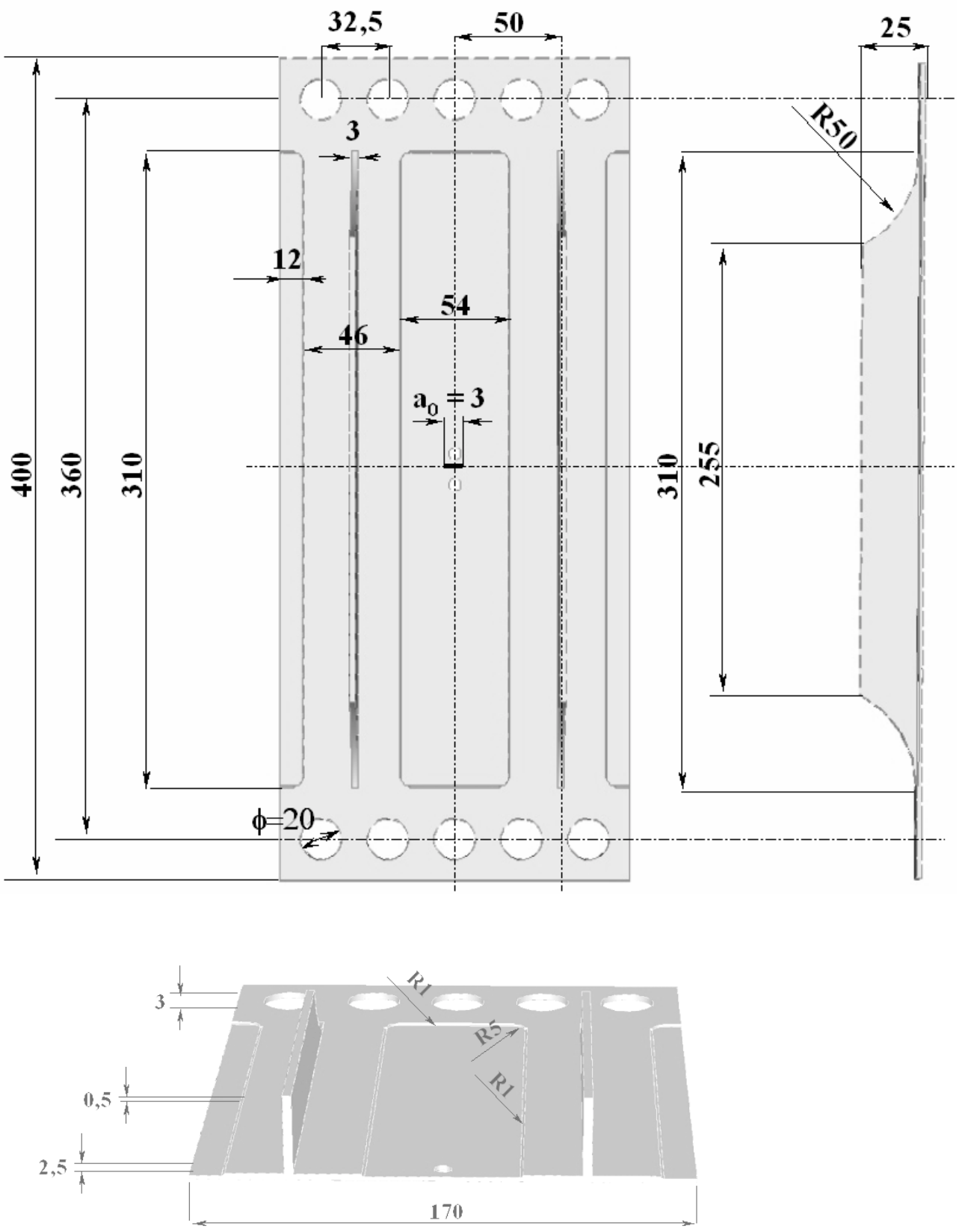

all dimensions in mm

Figure 4.11. Dimensions of the two stringer specimen (2SP)

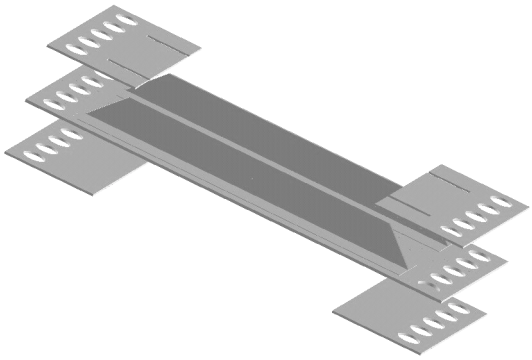

Figure 4.12. Location and form of the dopplers on the specimen. Their dimensions are plotted in Figure A.6

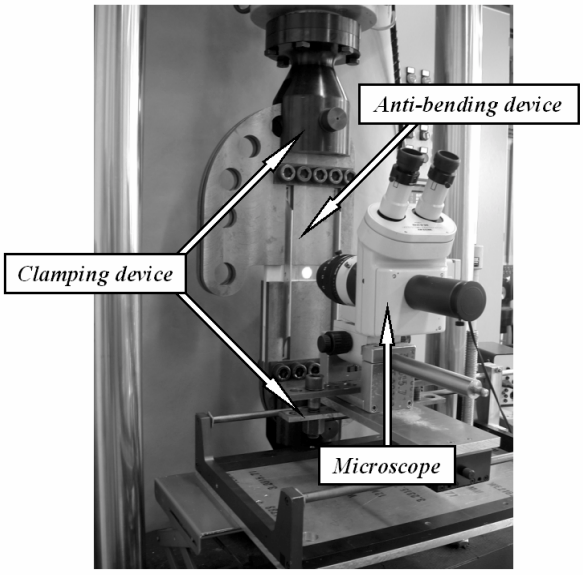

Figure 4.13. 2SP test-rig (reference DE03)

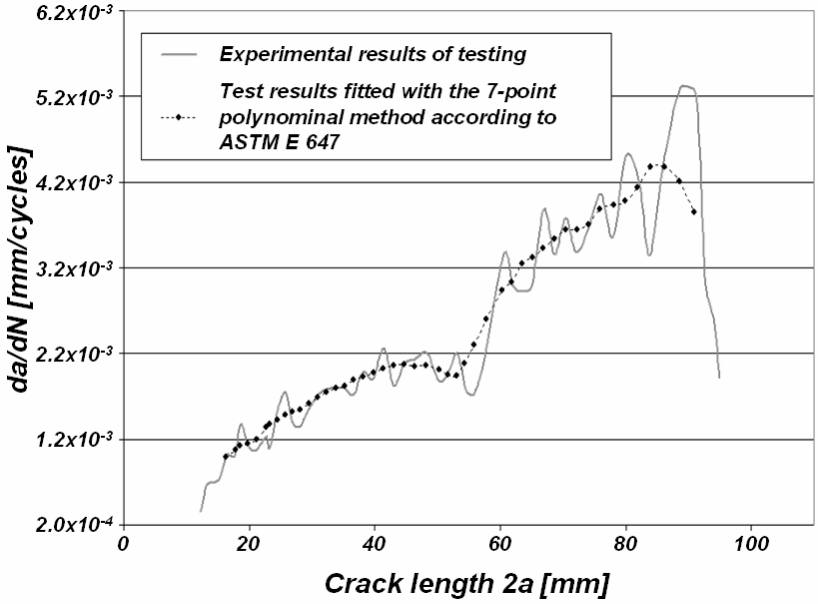

Figure 4.14. Crack growth versus crack length for the 2SP

The collected crack length data was stored with its corresponding number of cycles, *N*. Using these test data, the crack growth rate was calculated and plotted versus the crack length as illustrated in Figure 4.14. In this specimen the stress intensity factor amplitude, ΔK, cannot be calculated, as the geometric factor is unknown for such kind of structure. Therefore, the crack growth rate diagram (*da/dN* vs. ΔK) cannot be depicted.

In order to control the regime of crack propagation, a fractographic study by scanning electron microscopy was performed on different parts of the fractured surface. The results showed regular striations characteristic of fatigue during propagation until the stringer; however, as can be observed in Figure 4.15.b, a mixed behaviour of striations and ductile fracture took place by crossing the stringer.

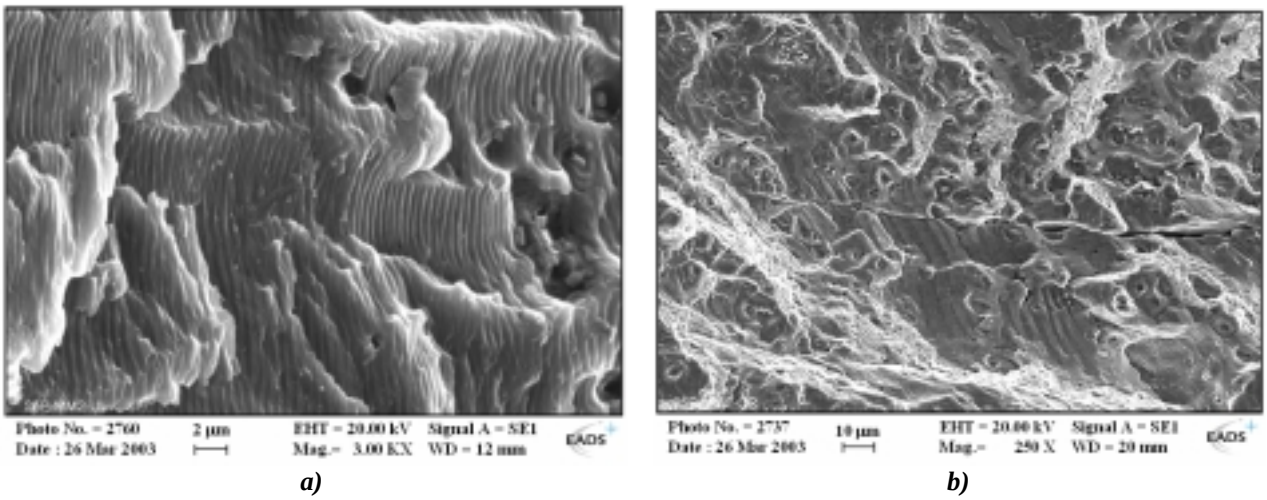

a) ***b)***

Figure 4.15. SEM images of the 2SP fractured surface at a) before the stringer and b) direct near the stringer

4.3.3 Crack turning specimens and tests

The Doubler Cantilever Beam is a specimen widely used in the analysis of crack turning, as introduced in section 2.5.3. Therefore, it was also used in this work to analyse both the crack turning behaviour on *AA* 2024-T3 and to evaluate crack turning criteria comparing test results with crack path predictions. Its geometry, plotted in Figure 4.16, was sized to allow about several centimetres of quasi-stable crack growth without excessive plasticity and to produce *T*-stresses similar in magnitude to those occurring in a pressurized fuselage as a crack approaches a stiffener [9, 23].

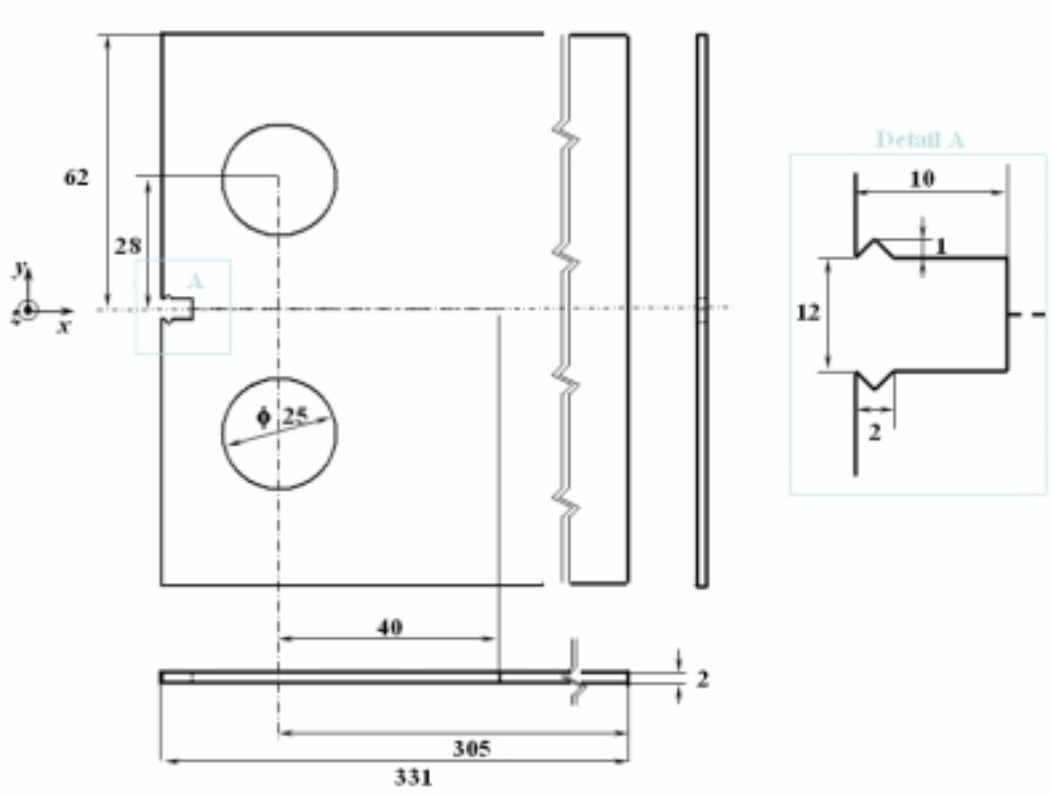

Figure 4.16. Dimensions of the DCB-specimen

Two different test sets were created. The first, referenced as RU04, was composed of 12 *DCB*-specimens with three different initial crack lengths of *40*, *90* and *140* mm. The purpose was to analyse the crack turning behaviour under:

a) three different K_I/T-ratios, i.e. with three different crack lengths,

b) two different pre-crack directions: parallel (T-L) and perpendicular (L-T) to the extrusion direction, and

c) two different loadings: quasi-static and cyclic loading.

These specimens were tested under assignment of AIRBUS by the Moscow State Aviation Institute (*MAI*) and the Central Aerodynamic Institute (*TsAGI*) in Russia. Three specimens with a crack length of *90* mm were tested under cyclic loading with a maximum force of *1.2* kN and a loading ratio, *R*, of *0.1*. The other nine, three for each crack length, were tested under quasi-static loading. Six of them were tested on the L-T direction and three on the T-L direction. This test-matrix is summarised in Table 4.6.

Table 4.6. Test-matrix for set reference RU04

Initial Crack length	*Direction*	*Quasi-static loading*		*Cyclic loading*	
40 mm	L-T	DCB_Static_40-LT	2x	-	0x
	T-L	DCB_Static_40-TL	1x	-	0x
90 mm	L-T	DCB_Static_90-LT	2x	DCB_Fatigue_90-LT	2x
	T-L	DCB_Static_90-TL	1x	DCB_Fatigue_90-TL	1x
140 mm	L-T	DCB_Static_140-LT	2x	-	0x
	T-L	DCB_Static_140-TL	1x	-	0x

The manufactured specimens were tested with an anti-bending device on a servo hydraulic machine. The crack was propagated from its original length to specimen failure. During the crack propagation the growth was monitored by means of a clip gauge mounted at the crack mouth to measure the crack opening displacement (*COD*) and also by means of a travelling microscope.

The collected *COD*-data was stored with its corresponding force for the quasi-static loading test. For the cyclic loading tests the crack length was recorded together with its lifetime *N*. After the test, the crack path was analysed by means of a microscope on both sides of the specimen. Figures 4.17 to 4.19 show the crack path results for a *40*, *90* and *140* mm notched specimen under quasi-static loading. Figure 4.20 shows the crack path results for a *90* mm notched specimen under cyclic loading. Figures 4.21 to 4.23 illustrate the stored values of *COD* and the applied force for *40*, *90* and *140* mm pre-cracked specimen under quasi-static loading.

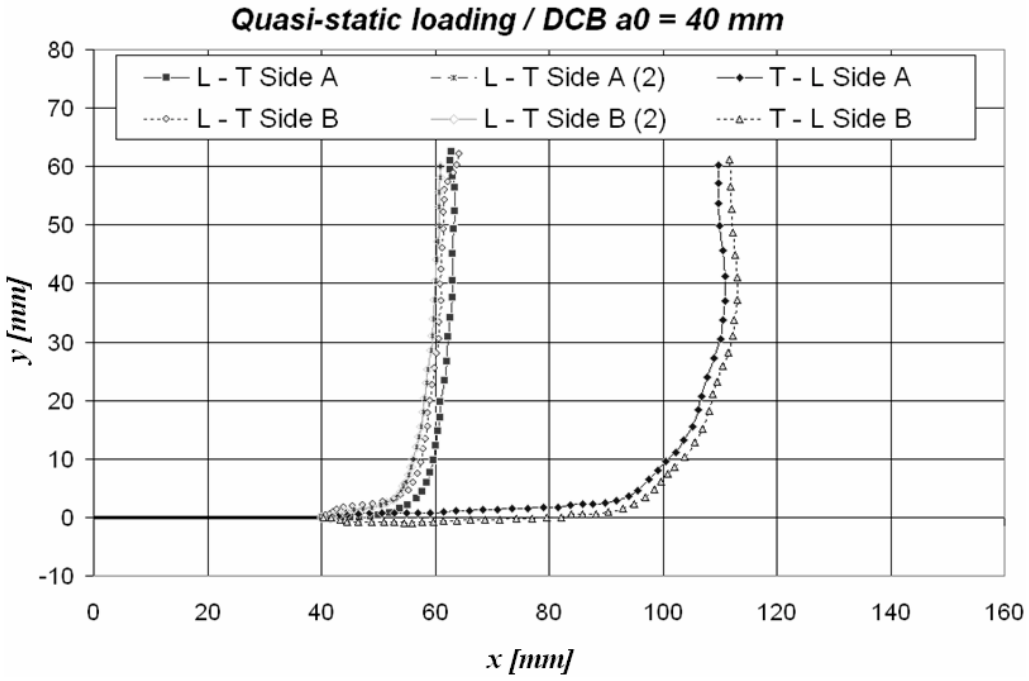

Figure 4.17. Crack path results for a 40 mm notched DCB under quasi-static loading

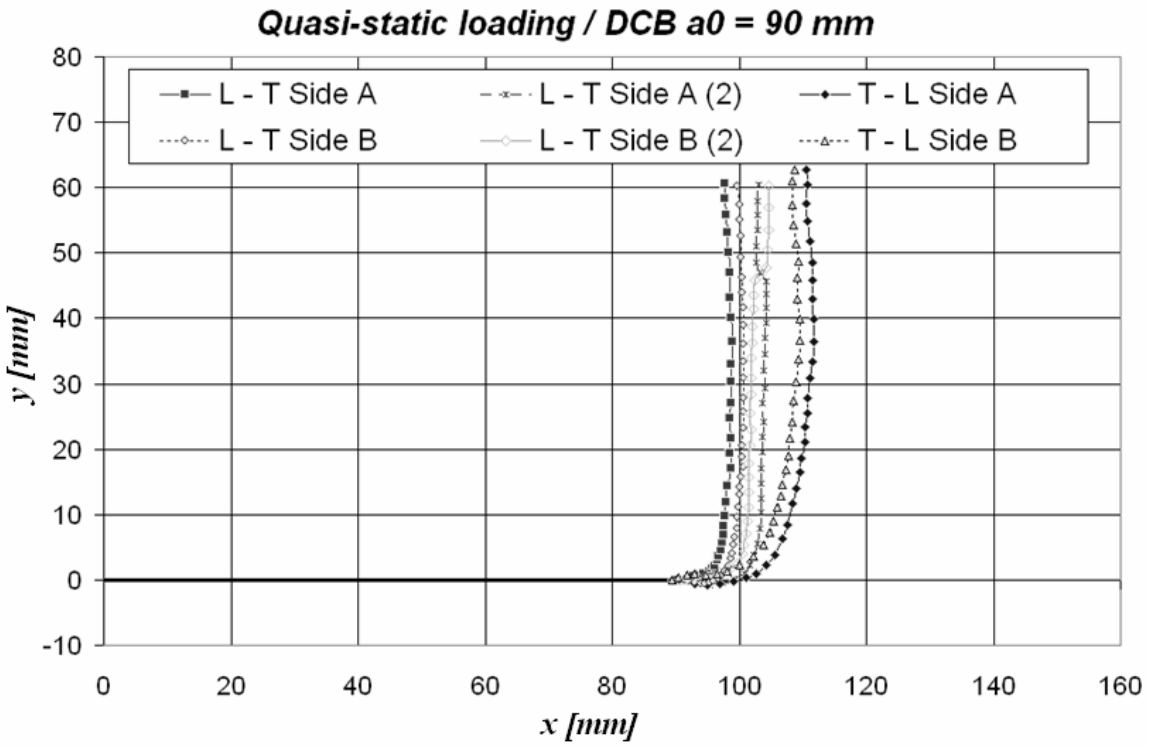

Figure 4.18. Crack path results for a 90 mm notched DCB under quasi-static loading

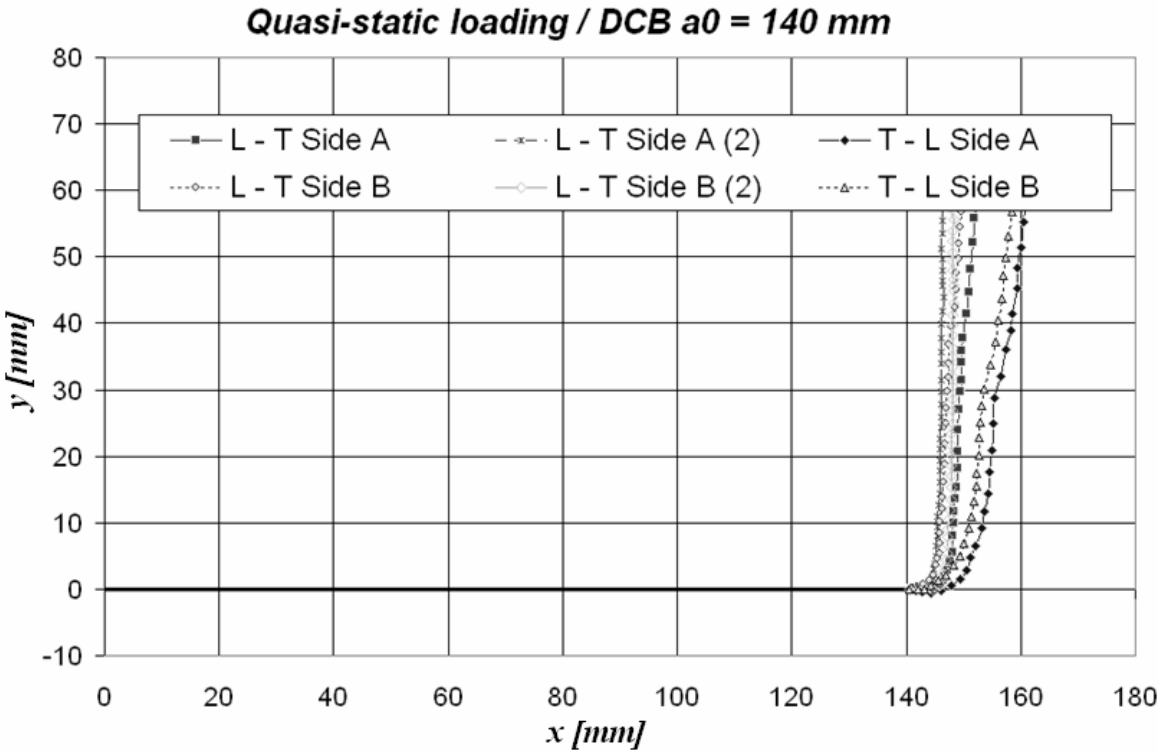

Figure 4.19. Crack path results for a 140 mm notched DCB under quasi-static loading

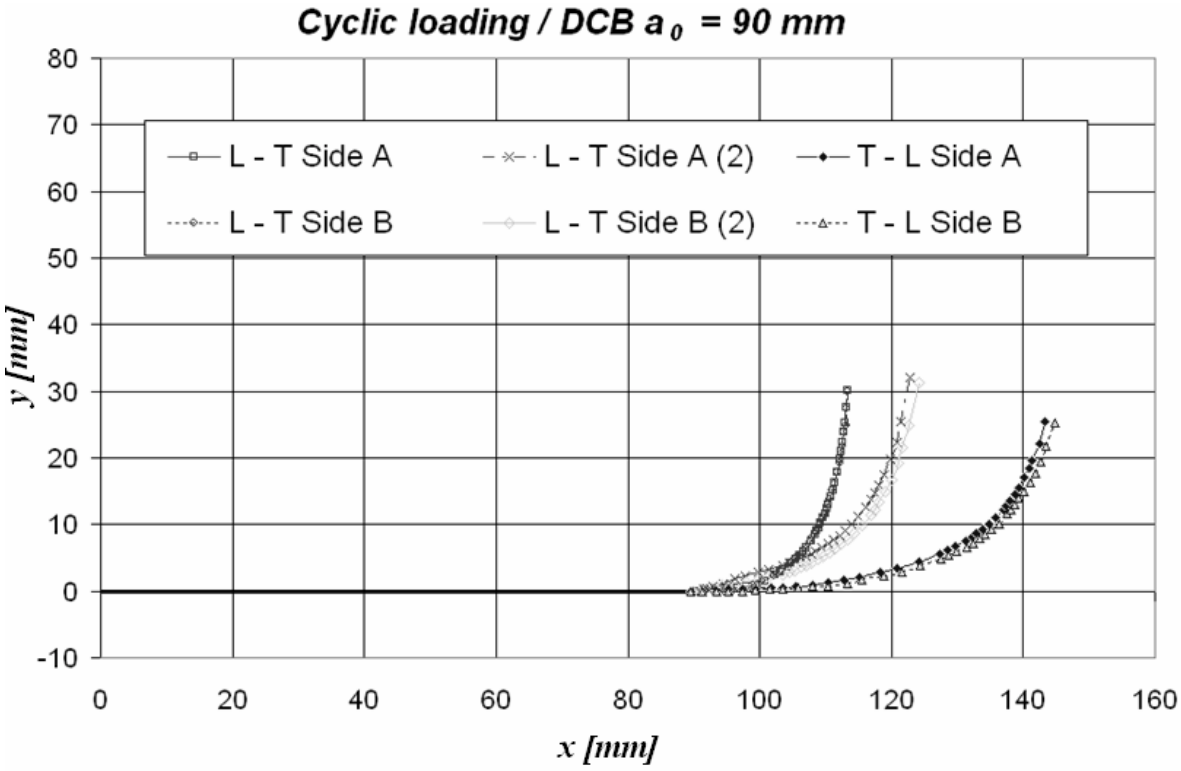

Figure 4.20. Crack path results for a 90 mm notched DCB under cyclic loading

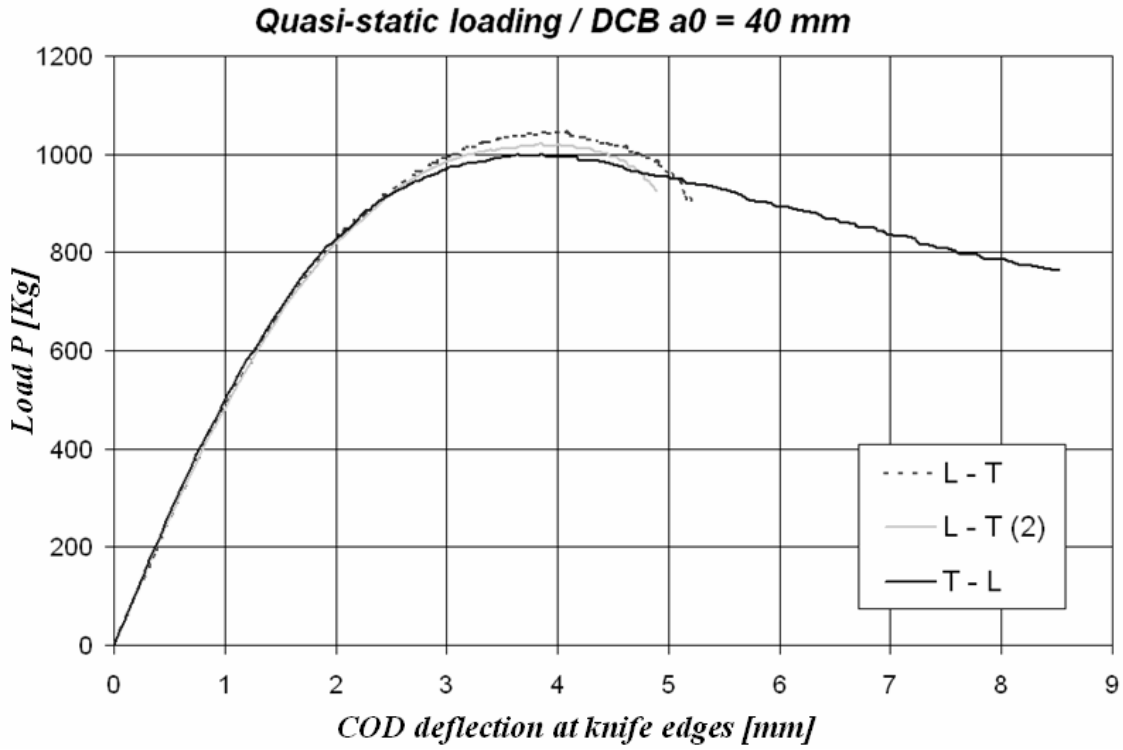

Figure 4.21. Applied load vs. COD results for the DCB with 40 mm notch and under quasi-static loading

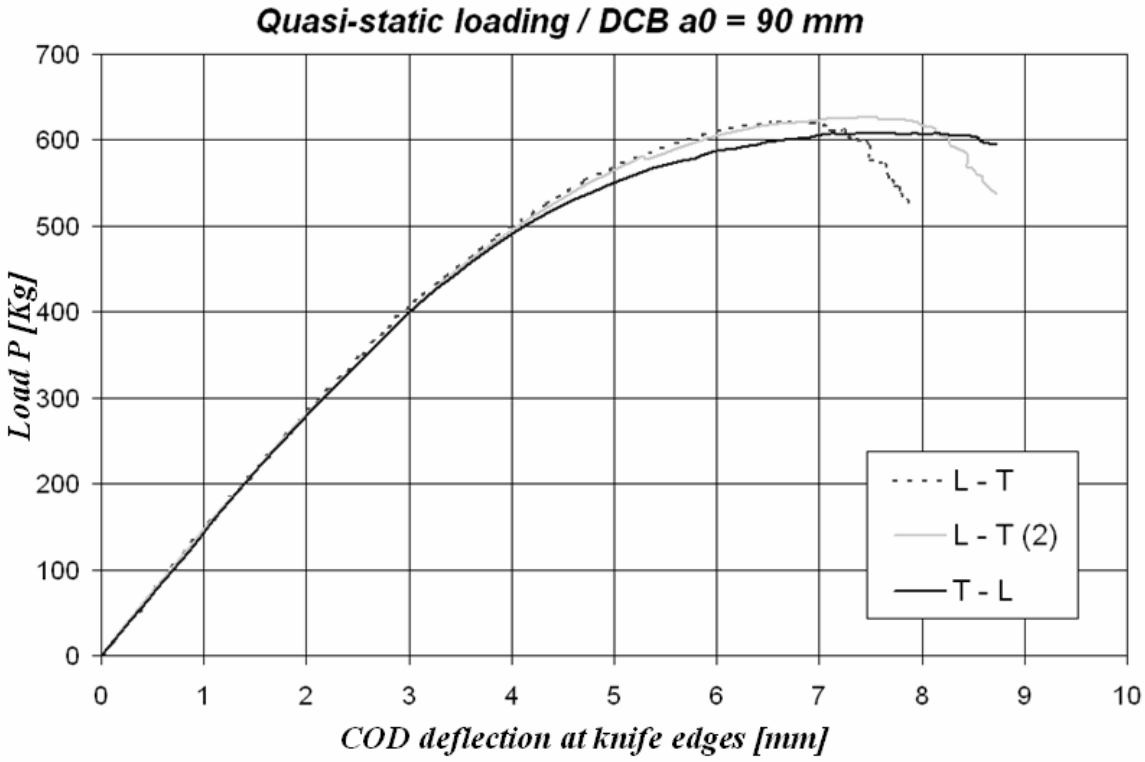

Figure 4.22. Applied load vs. COD results for the DCB with 90 mm notch and under quasi-static loading

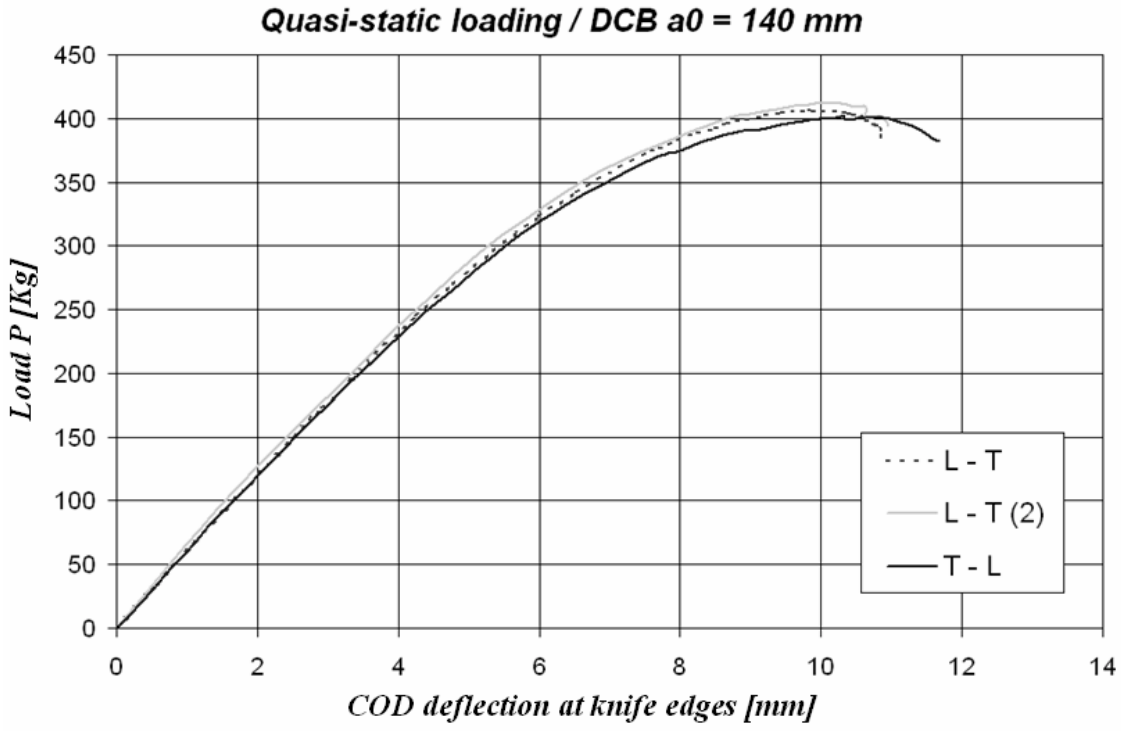

Figure 4.23. Applied load vs. COD results for the DCB with 140 mm notch and under quasi-static loading

In order to be able to simulate the crack propagation under quasi-static loading, the applied force for each crack length is needed as input. However, there was no such information recorded from this set of testing (RU04). Nevertheless, the lack of this information was generated by means of simulations.

A second *DCB*-test set, set reference DE05, was created in order to clarify some observations arising from this last tests and first simulation results. Eleven specimens were machined with the same geometries as in Figure 4.16, with three different notch lengths in L-T direction: one with *33* mm, two with *38* mm, and six with *43* mm. Eight of them were notched with a saw cut, producing a notch thickness of *1.5* mm. The others were notched by means of the electro-erosion technique, manufacturing a notch of thickness equal to *0.3* mm. The angles between surface of the notch and the normal of the specimen surface, ψ, described in Figure 4.24, were *0°* for two of them and *45°* for the rest. Five specimens were tested under quasi-static loading and the three left under cyclic loading. This test-matrix is summarised in Table 4.7.

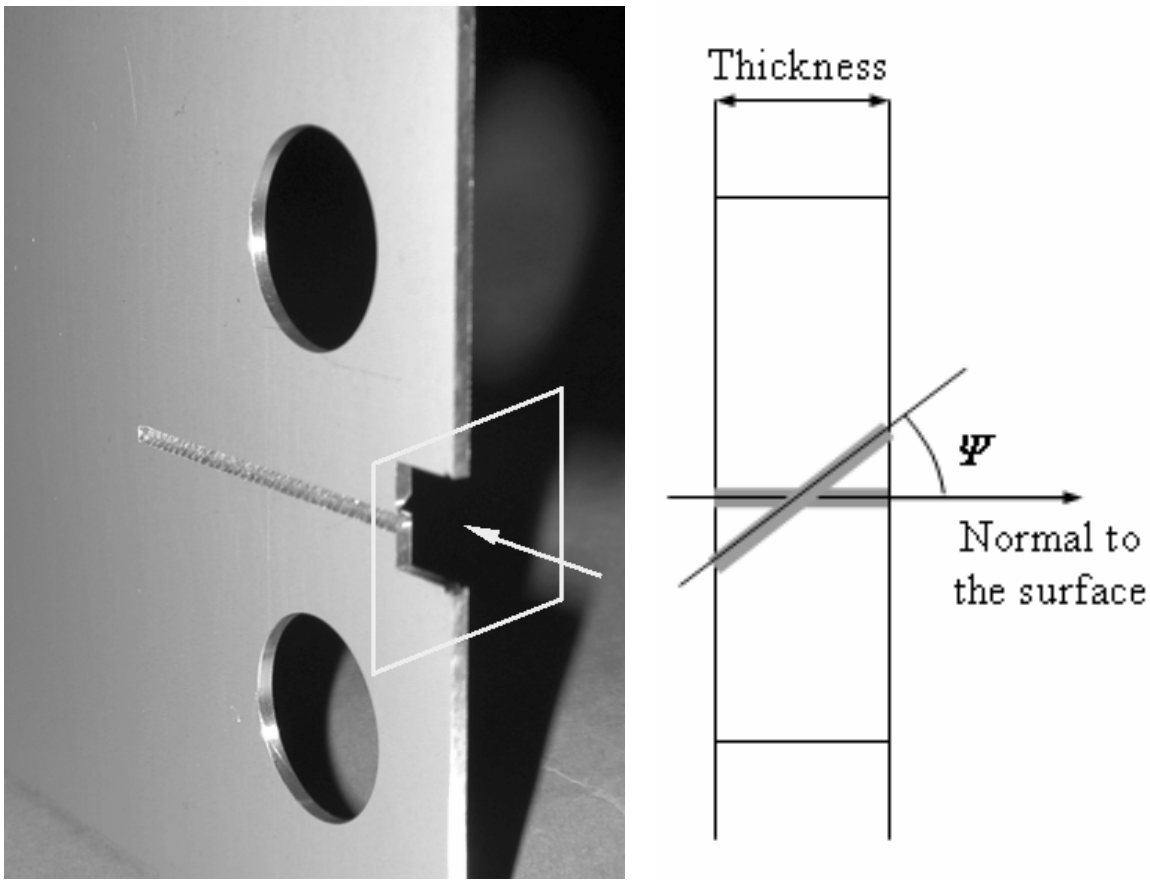

a) ***b)***

Figure 4.24. a) DCB-specimens corresponding to the set reference DE05 b) definition of the notch angle Ψ

Table 4.7. Test-matrix for set reference DE05

Load	*Specimen*		*Initial notch length [mm]*	*Notch*	
				Angle-ψ	*h_c [mm]*
Quasi-static loading	DCB_S4540	2x	43	45°	1.5
	DCB_S4535	1x	38	45°	1.5
	DCB_S4530	1x	33	45°	1.5
	DCB_S040_hc15	1x	43	0°	1.5
	DCB_S040_hc03	1x	43	0°	0.3
Cyclic loading	DCB_F4540	2x	43	45°	1.5
	DCB_F4535	1x	38	45°	1.5

With this set of testing, it was intended to analyse the influence of the starting notch and the notch angle, ψ. A redesign of the clamping device was performed to avoid any friction influence. Hence, a cylinder bearing was introduced as illustrated in Figure 4.25.

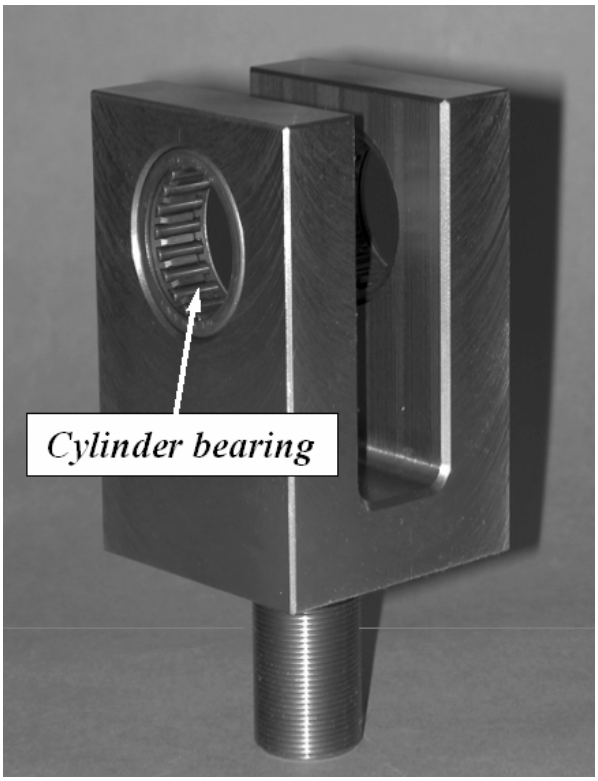

Figure 4.25. Clamping device including cylinder bearing

The manufactured specimens were tested with an anti-bending device on the servo hydraulic machine, INSTRON® Model 8032. A support was introduced at the end of the anti-bending device in order to prevent the influence of its weight on the results. The crack was propagated from its original length to specimen failure. The crack growth was monitored by means of the crack opening displacement and a travelling microscope, as illustrated in Figure 4.26. The applied cyclic loading ratio was *0.1* and two different maximal loads were used: *1.2* and *1.8* kN.

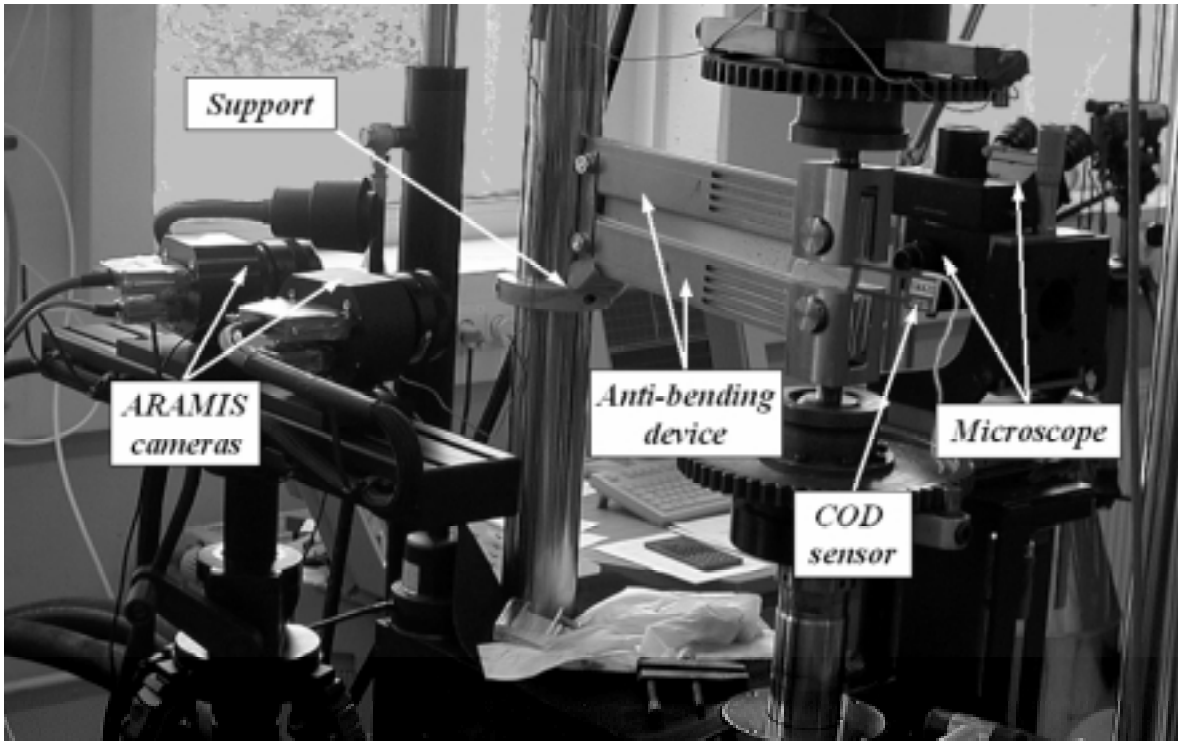

Figure 4.26. Test-rig for set reference DE05

Figures 4.27 and 4.28 show the obtained crack path results for the cyclic and quasi-static tests on the *DCB*-specimens defined in Table 4.7.

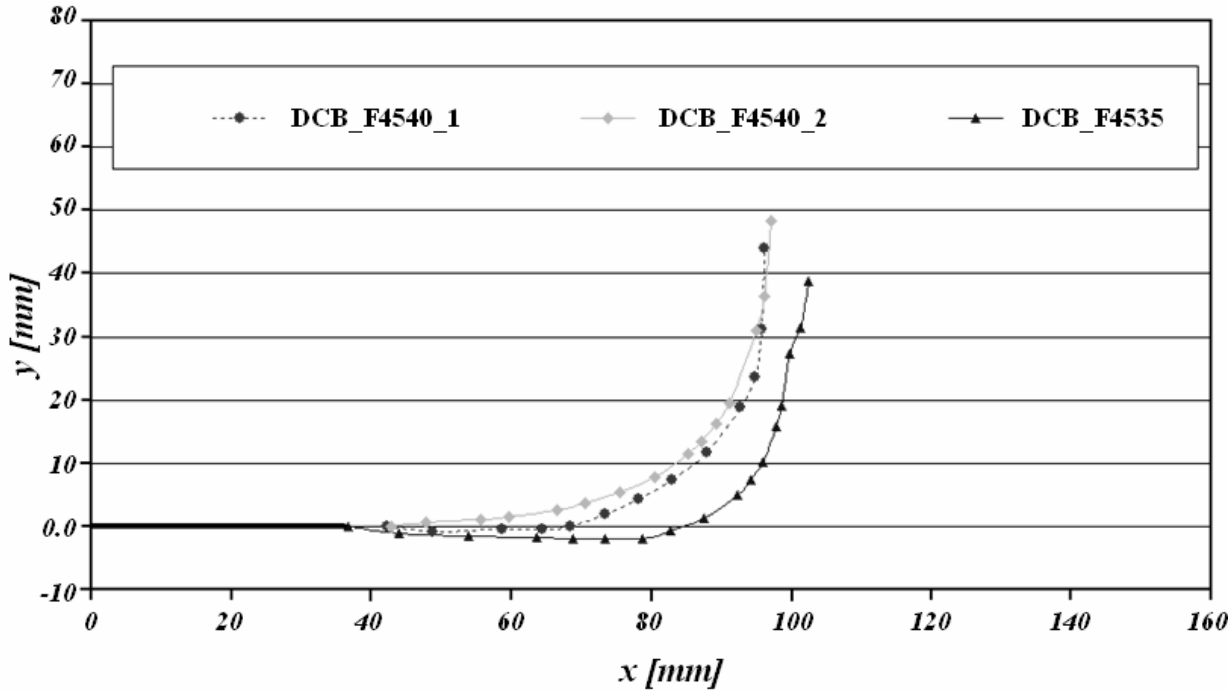

Figure 4.27. Crack path results for the DCB under cyclic loading (reference DE05)

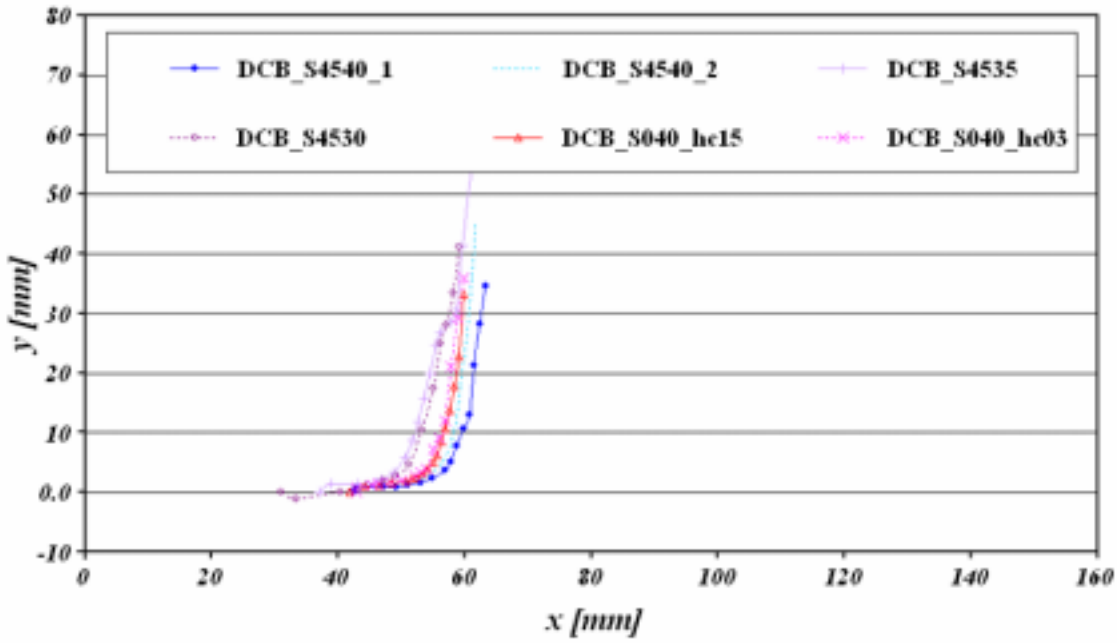

Figure 4.28. Crack path results for the DCB under quasi-static loading (reference DE05)

Four of these *DCB*-specimens were analysed by means of ARAMIS to control the crack tip plasticity dimensions. These were prepared before the test with a stochastic or regular pattern onto the surface of the specimen by means of a spraying technique as illustrated in Figure 4.29.a. Figure 4.29.b shows the position of the first and last recognised and stored patterns (or points). The results of the strain calculations are depicted in Figure 4.30 for the cyclic loading and in Figure 4.31 for the quasi-static loading.

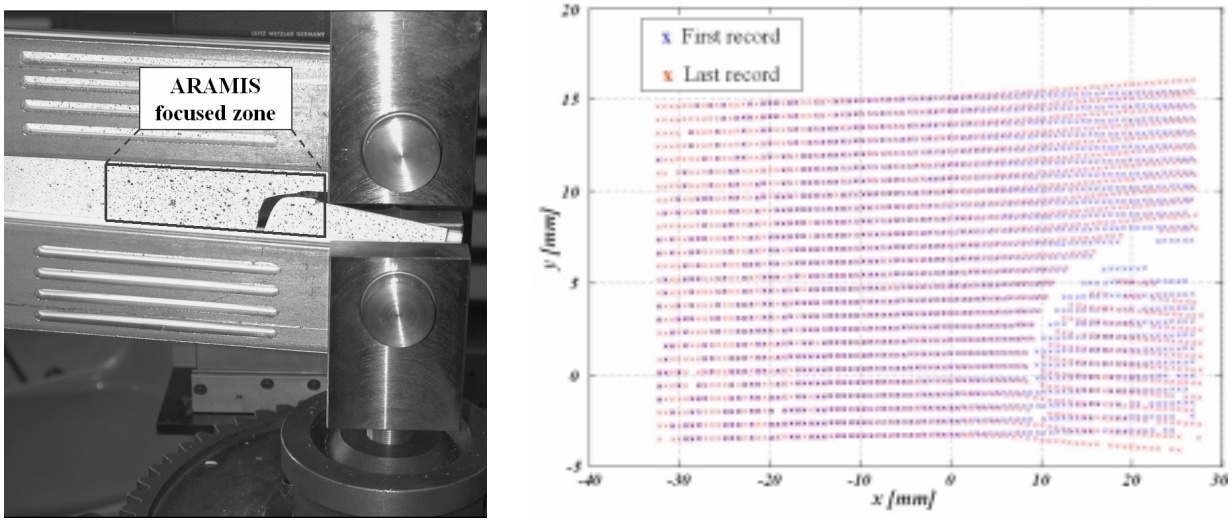

a) *b)*

Figure 4.29. ARAMIS analysis a) focused zone b) graphical representation of the output data. (data worked with Matlab®)

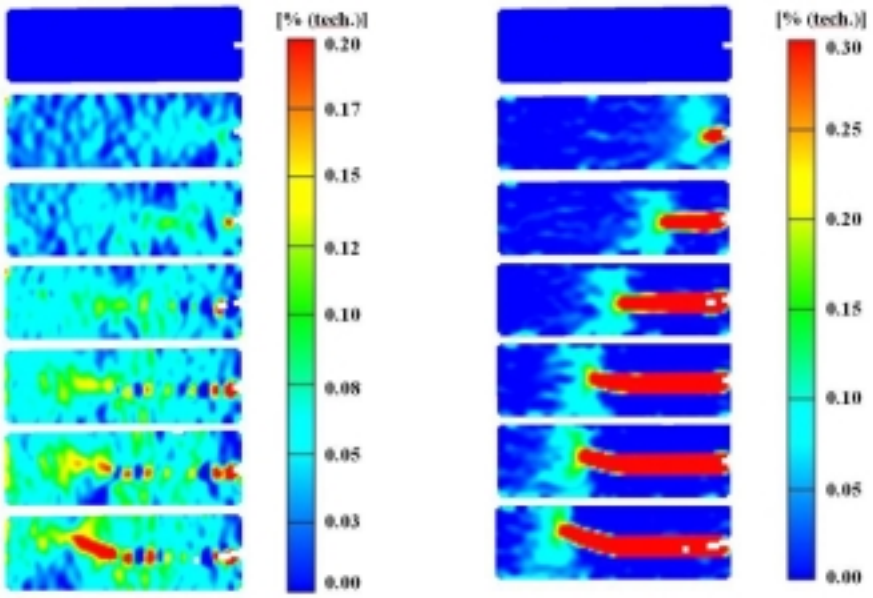

Strain in x direction ***Strain in y direction***

Figure 4.30. ARAMIS strain analysis. Cyclic loading. DCB_F4540_1

On these tests (DE05) the correspondence between *COD*, applied force and crack length were stored for *12* different crack lengths during the crack propagation under quasi-static loading. This allowed the evaluation of the modelling procedure used on the evaluation of the results of testing of ref. RU04 to find out the association between crack length, applied force and *COD*, sections 6.1.1 and 6.3.2.

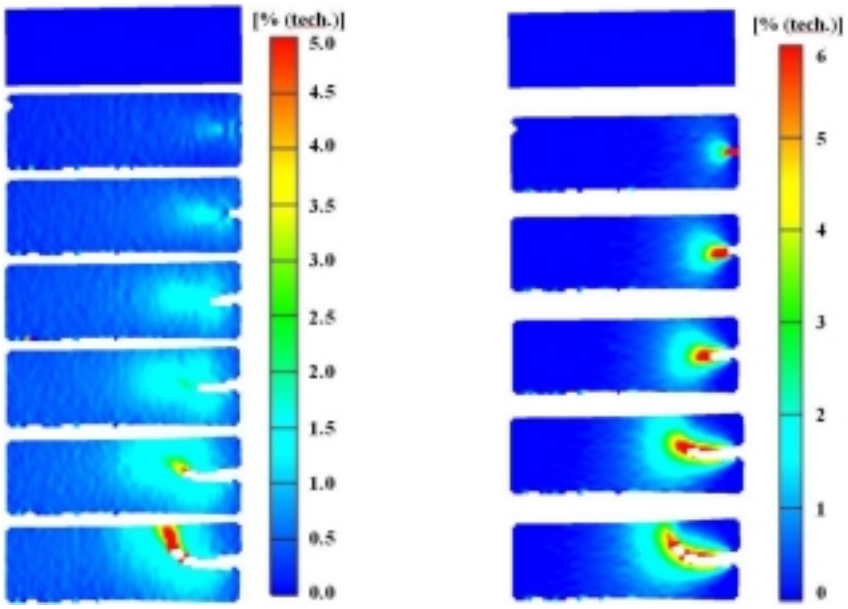

Strain in x direction ***Strain in y direction***

Figure 4.31. ARAMIS strain analysis. Quasi static loading. DCB_S040_hc03

The first objective for using the cruciform specimen (reference RU06) was to analyse the crack turning behaviour under different biaxial stress ratios. It is common in aeronautics to have structures under biaxial stress, e.g. the two crack scenarios depicted in Figure 3.1. Nevertheless, only the result of one specimen was available. The *CFS* was then analysed by means of the *FE*-tool. Here, the effect of model simplicity, non-alignment of the applied loading on the crack path prediction and crack tip perturbations were analysed.

The dimensions of the tested *CFS*-specimen are plotted in Figure 4.32.a. Its initial crack length, *2a*, was *150* mm in L-T direction and the stresses in the *x*-axis, parallel to the notch, and the *y*-axis, perpendicular to the notch, were *75.32* and *107.6* MPa respectively.

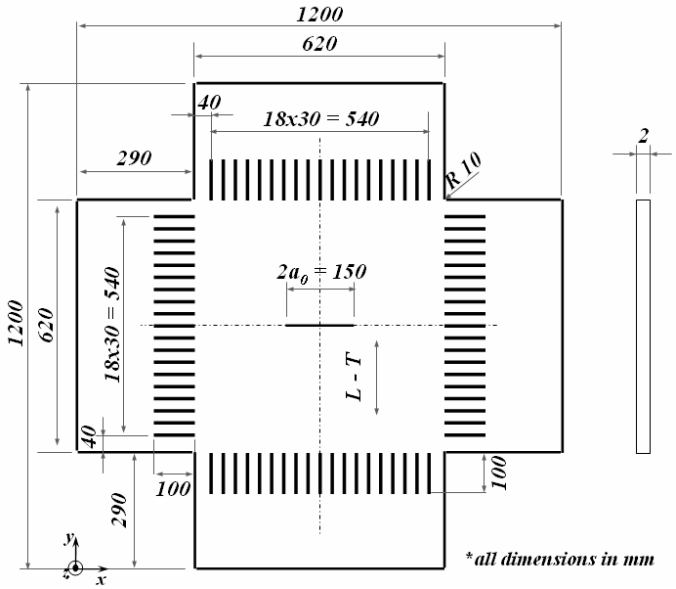

a)

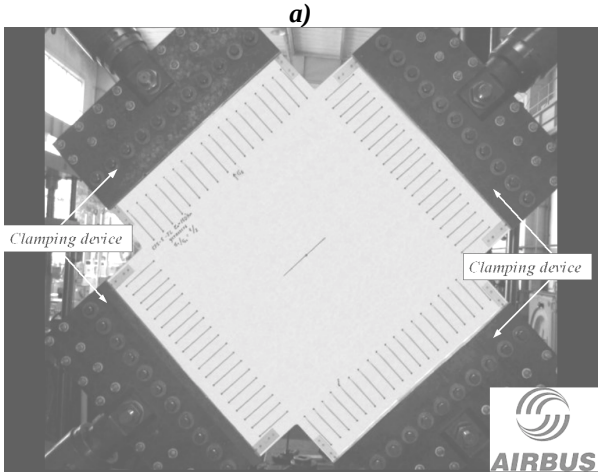

b)

Figure 4.32. a) Dimensions and b) test-rig of the CFS-specimen (reference RU06)

This specimen was tested under assignment of AIRBUS by *MAI* and *TsAGI* in Russia. The applied cyclic loading ratio was *0.1* and the testing frequency was *1* Hz. The crack was monitored as a function of the number of cycles. The resulting crack path and crack length versus life time are depicted in Figure 4.33.

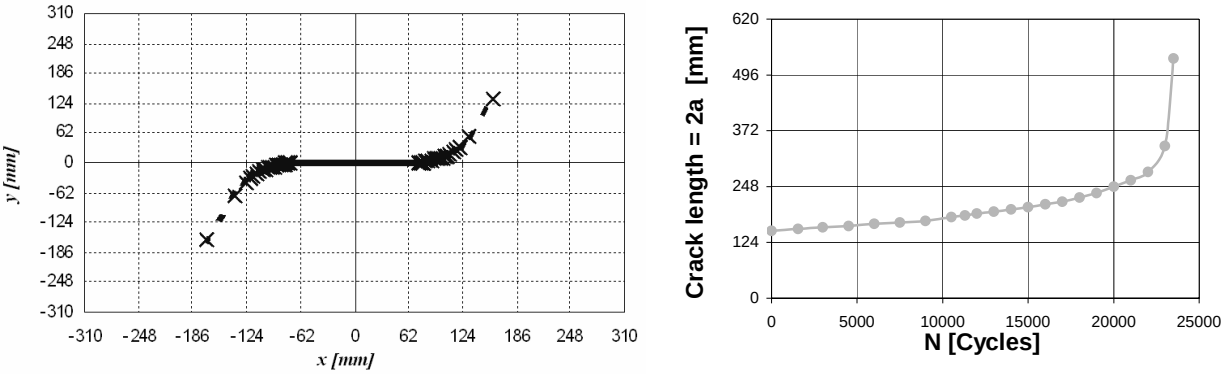

a) ***b)***

Figure 4.33. Results of testing for the CFS-specimen (reference RU06) under cyclic load conditions a) obtained crack path and b) a vs. N

An overview of all tests performed during this work is found in Table 4.8.

Table 4.8. Test-matrix summary

Specimen	***Test type***	***Set reference***	***Thickness [mm]***	***Directions***	***Specimens pro direction***
Dog-bone	***Tensile stress***	DE01	2	L, 45°, LT	3x
MT	***Fatigue crack growth***	DE02	1.6	L-T, 45°, T-L	5x
			2.5	L-T, 45°, T-L	4x
	Residual strength		1.6	L-T, 45°, T-L	3x
2SP	***Fatigue crack growth***	DE03	2.5-3-25*	L-T	2x
DCB	***Fatigue crack growth***	RU04 and DE05	2	T-L	1x
				L-T	5x
	Residual strength		2	T-L	3x
				L-T	12x
CFS	***Fatigue crack growth***	RU06	2	L-T	1x

**The different thicknesses correspond to shell, pocketing and stringer (Figure 4.11)*